UNCLASSIFIED

Inactive [redacted]

Copy No. 44
RM No. SI8I09

NACA

RESEARCH MEMORANDUM

for the

Bureau of Aeronautics, Department of the Navy

LABORATORY INVESTIGATION OF TWO AUTOPILOTS FOR A $\frac{1}{10}$-SCALE DROP MODEL OF THE GRUMMAN F8F-1 AIRPLANE - TED NO. NACA 2466

By

Jerome M. Teitelbaum and Ernest C. Seaberg

Langley Aeronautical Laboratory
Langley Field, Va.

NATIONAL ADVISORY COMMITTEE FOR AERONAUTICS

WASHINGTON

UNCLASSIFIED

NACA RM No. SL8I09

NATIONAL ADVISORY COMMITTEE FOR AERONAUTICS

RESEARCH MEMORANDUM

for the

Bureau of Aeronautics, Department of the Navy

LABORATORY INVESTIGATION OF TWO AUTOPILOTS FOR A $\frac{4}{10}$-SCALE DROP MODEL OF THE GRUMMAN F8F-1 AIRPLANE - TED NO. NACA 2466

By Jerome M. Teitelbaum and Ernest C. Seaberg

SUMMARY

Performance investigation and frequency response analyses were conducted on two autopilot control systems designed for use in the $\frac{4}{10}$-scale model of the Grumman F8F-1 airplane. The first system, based on the action of a displacement gyroscope only, was investigated to find the cause of a small-amplitude pitch oscillation which had been noted in previous flight tests. The results of the investigation conducted revealed that, although the autopilot-model combination was dynamically stable, a hunting oscillation was possible due to a change in autopilot characteristics in a dive. This hunting condition can be eliminated by increasing the gyroscope pickoff dead spot without greatly reducing dynamic stability of the autopilot-model combination.

The second system based on the combined action of displacement and rate gyroscopes was tested to determine the autopilot characteristics desirable and to predict the control-surface linkage ratios required for dynamically stable flight. The results of the tests conducted show that satisfactory autopilot characteristics can be obtained by selective mixing of the signals from the displacement gyroscope, the rate gyroscope, and the feedback system. By using this adjusted autopilot and by selective gearing between the control surface and the servomotor, conditions for stable flight based on the frequency response analysis can be predicted.

A comparison of the two autopilot systems shows that slight improvement in the dynamic stability of the model can be expected when the second system mentioned above is used.

INTRODUCTION

At the request of the Bureau of Aeronautics, Department of the Navy, the NACA conducted oscillating-table tests on two separate autopilots designed and constructed by the Naval Air Experimental Station, Philadelphia, Pa., for use in the $\frac{4}{10}$-scale Grumman F8F-1 drop model in order to stabilize and program the flight of the model. In the first autopilot (to be referred to as system 1), the problem involved was to determine the cause of the oscillatory flight tendencies of the model during the diving portion of flight. The investigation conducted was based on an examination of the following:

1. Effect of signal pressure cut-off

2. Signal pickoff dead spot

3. Stability analysis of the autopilot-model combination

4. Effect of dive angle on the autopilot response

5. Effect of a roll oscillation on pitch and yaw controls

In the second autopilot (to be referred to as system 2), the problem was to determine the effect of the rate gyroscope, the displacement gyroscope, and the servomotor damping on the autopilot, and to predict the control-surface linkage ratios required for dynamic stability of the autopilot-model combination. The tests conducted consisted mainly of frequency-response table tests in which the signal strengths of the component parts were varied. As the autopilot was constructed identically in all three planes (that is, pitch, yaw, and roll), the tests were conducted in pitch only with and without simulated air load on the servo and the results applied to all three motions. All tests were made by the Pilotless Aircraft Research Division of the Langley Aeronautical Laboratory.

SYMBOLS AND DEFINITIONS

K	control-amplitude ratio (ratio of control deflection to airplane displacement)
K_m	control-amplitude ratio obtained from solution of aerodynamic equations of motion
K_p	control-amplitude ratio obtained from oscillating-table tests of autopilot

[redacted]

ϵ phase angle, degrees (positive indicates lead of δ ahead of θ)

ϵ_m phase angle obtained from solution of aerodynamic equations of motion, degrees

ϵ_p phase angle obtained from oscillating-table tests of autopilot, degrees

ω angular frequency of oscillation, radians per second

θ angle of pitch, degrees

ϕ angle of bank, degrees

ψ angle of yaw, degrees

δ_e elevator deflection, degrees

δ_a aileron deflection, degrees

δ_r rudder deflection, degrees

V true airspeed, feet per second

Hunting - a self-excited steady-state oscillation

Gyro pickoff - the part of a gyro unit which detects the error between gyro reference and airplane attitude and supplies the corrective signal to the servo

Dead spot - the angle included within the limits of gyro displacement which results in no servo motion

Control-surface linkage ratio - the ratio of the angular deflection of the control surface to the angular rotation of the servo arm

Cross coupling - the response of an autopilot mechanism in one plane to a disturbance of the model in another plane

APPARATUS

The two autopilot control systems tested were mounted on trays and were supplied by the Navy Department.

[redacted]

System 1

This system consists of three air-driven Diehl Directional Gyros and three Lear Linear Actuators, model 420AR. The setup used is similar to the one shown in figure 1 and described in reference 1. A schematic representation is shown in figure 2. Although the autopilot is a three-axis system, only one axis is outlined.

Movement of the servos (actuators) which operate the elevators, ailerons, and rudder is controlled by pneumatic electrical gyro pickoffs. Gyro displacement moves a cut-off plate between a jet and orifice type pressure feed to the pickoff. The pressure variation due to the position of the plate causes movement of a spring-loaded diaphragm. The diaphragm controls the motion of a switch arm between two contacts which, in turn, energize a pair of relays that engage and control the direction of motion of the constant-speed servos. The gyro cut-off plate is so constructed that either a fast or slow rate of change in pickoff pressure with gyro displacement can be selected, as shown in figure 2. The dead spot is adjusted by changing the spacing between the contacts in the pneumatic electrical pickoff.

The follow-up system is superimposed on the gyro pickoff by means of a cable linked between the servo and a pulley geared to the pickoff orifice. Movement of the servomotor due to the gyro displacement causes the orifice in the pickoff to move in the direction of the gyro displacement. This motion continues until the air pressure in the orifice is such that the switch arm breaks contact and the servo disengages. By this method, servo motion becomes proportional to the amount of gyro displacement. The dive mechanism consists of a means of varying the active length of the follow-up cable, thus moving the pick-up orifice or base reference location to give the desired dive or climb.

System 2

This system is composed of three air-driven Diehl displacement gyros, three Pioneer, P-1, rate gyros, and three Pioneer two-phase, induction-type rotary servos geared to give the required torque output. The autopilot containing the gyros and amplifier is shown in figure 3. A block diagram showing the operation of one axis of the autopilot is contained in figure 4. Four-hundred-cycle autosyn pickoffs are used to detect both displacement and rate errors. In order to vary the rate and displacement response sensitivities of the autopilot, three controls are added to the system for each plane of motion, a "rate" control varies the effect of rate error on the system, a "range" control varies the effect of the displacement gyro, and the "follow-up" control varies the amount

of servomotor damping. The output from each pair of gyros (that is, one rate and one displacement gyro for each plane of motion) is fed through an electronic amplifier, which is electrically connected to the servomotor. A 400-cycle autosyn pickoff is geared to the servomotor and furnishes feedback signal. The strength of the feedback signal as compared with the signals from the gyros is a measure of the effective servo damping. The output of an inverter supplies the electrical power necessary to drive the rate gyro motors, autosyn pickoffs, amplifier, and servomotors.

The system operates as follows: As the model moves off course, the autosyn pickoffs on one pair of gyros are displaced with respect to their gyro axis. This causes electrical signals to be sent to the rate and range control, which are preset. From the rate and range control, the combined signal travels through the amplifier and energizes the servomotor, causing control-surface displacement at a speed proportional to the strength of the input signal. Movement of the servomotor also causes the autosyn pickoff in the servomotor housing to be displaced and feedback to the follow-up control, a signal which is opposite in sign to the signal produced by the gyros. Movement continues until these two signals equalize each other, thus giving proportionality between the displacements of the gyros and servo motion.

Equipment

An oscillating table capable of producing sinusoidal oscillations up to 5 cycles per second and with amplitude adjustment up to $\pm 15^{\circ}$ was used to obtain data for the frequency-response tests. A position recorder was attached to the table and a similar one attached to the servo in order to record table motion and servo position as functions of time.

PROCEDURE

System 1

The entire autopilot system was mounted on a tray and attached rigidly to the oscillating table in a position so that the motion of the table would simulate a sinusoidal pitch oscillation of the airplane. The frequency response of the autopilot system was obtained by oscillating the table at various amplitudes and frequencies and recording the table displacement and servo motion as functions of time. Dead spot was measured by disconnecting the servo and recording table displacement and power to the servo. Dead spot, in degrees, was obtained as the difference in table position required for signal reversal to the servo. The tests to determine the effect of the dive mechanism were conducted by uncaging the gyro in the level position and rotating the table approximately 15° at various

displacement rates at the same time as the dive mechanism was energized. Cross-coupling tests were conducted by mounting the autopilot on the oscillating table to simulate rolling of the model and recording the roll position and motion of the pitch servo due to the roll displacement. The tests were conducted with the pitch displacement gyro signal pickoffs in both the normal and wide-open positions.

System 2

The autopilot tray containing the displacement and rate gyros, amplifier, and rate, range, and follow-up controls was attached to the oscillating table to simulate the pitching oscillation of the model. The servomotor, inverter, and air filter were mounted on an adjacent table and connected to the autopilot as shown in figure 5. The air load on the servomotor was simulated with a shock-cord arrangement, whereby 8 to 12 foot-pounds of resisting torque were applied to the servomotor upon movement of the servomotor arm in either direction from centered position. The arrangement used is shown in figure 5. Oscillating-table tests were conducted at various table amplitudes and frequencies and with various group settings of the rate, range, and follow-up controls. The effect of air load was determined by conducting some of these tests with and without simulated air loads and comparing the results.

RESULTS AND DISCUSSION

System 1

This system, based on the action of a displacement gyro only, was investigated to find the cause of a small-amplitude pitch oscillation which had been noted in previous flight tests. The tests were conducted without simulated air load as this load is not sufficient to affect the operation of the servomotors. The results of the tests conducted to determine the cause of the oscillation noted are as follows:

Signal pressure cutoff.- The tests were conducted with the slow rate of change of pickoff pressure with displacement only as attempts to use the fast rate produced hunting servo oscillations under all conditions.

Signal pickoff dead spot.- The dead-spot measurements using the slow rate of change of pickoff pressure cutoff were recorded as follows: Pickoff normal operating conditions, 1.4° and pickoff wide-open condition, 2.2°.

Stability analysis.- By application of the frequency-response method outlined in reference 2 and using the aerodynamic data given

in reference 3, the longitudinal stability of the autopilot-model combination was determined for a control-surface gearing of 3.75° control deflection per inch servo travel and for model velocities of 300 and 850 feet per second. The results of the tests with the pickoff set in the normal operating position are shown in figure 6, in which control-gearing ratio K and phase angle ϵ are plotted against angular frequency ω in radians per second. The results of the tests with the pickoff set in the wide-open position are shown as frequency-response curves in figure 7. Although some variation in characteristics was noted between the two tests, an analysis of the results obtained showed that in both tests the autopilot-model combination was stable for oscillations having amplitude of approximately ±9°, ±7°, ±4°, and ±2° and that, in flight, the model should damp to a value below ±2°.

Dive effect.- The results of the tests for dive condition with the dive mechanism in operation and with the dive mechanism inoperative are plotted in figure 8 for normal pickoff position and figure 9 for wide-open pickoff position. The tests were conducted at various autopilot displacement rates in order to cover the possible rate of change in airplane displacement that may be encountered in actual flight of the model, as this procedure was simpler than trying to calculate the theoretical flight path of the model. The results show that, with the pickoff in normal position, a hunting control oscillation became apparent at the end of the dive, while setting the pickoff in the wide-open position eliminated this oscillation. The hunting oscillation noted after a dive with the pickoff in normal position was due to the fact that the servomotor continued to coast after the pickoff signal stopped. This overshoot caused the follow-up system to change the orifice pressure in the pickoff to the extent that the spring-loaded diaphragm moved and closed the contact, giving reverse signal to the servomotor. No explanation as to why this hunting existed only after a dive could be found. With the contacts in the wide-open position, movement of the diaphragm was not sufficient to close the contact which previously gave reverse signal to the servomotor and started servo hunting.

Cross coupling.- With the pickoff in normal position (dead spot, 1.4°), no control oscillation in the pitch sense was noted due to roll until an outside source initiated a disturbance of the follow-up pulley. After this disturbance occurred, the servo control continued to oscillate at the same frequency as the forced roll oscillation. With the pickoff in the open position, it was not possible to obtain a coupled oscillation of pitch control due to roll oscillation. Figure 10 is a plot of the results of the tests showing pitch-control motion due to a roll oscillation of $6\frac{1}{2}^\circ$ at frequencies of $\frac{1}{2}$, 1, and $1\frac{1}{2}$ cycles per second with the pickoff in normal position and with an outside source initiating a disturbance of the follow-up pulley. Although the tests conducted

measured the pitch-control response to a roll oscillation, preliminary tests were made and similar coupling appeared to be present between all planes.

System 2

This system employing the use of a rate gyro in addition to the displacement gyro used in system 1 and having a proportional servo in place of a constant-speed control actuator was tested to determine whether or not improved flight characteristics could be expected with this autopilot-model combination. The results of the tests conducted are as follows:

Effect of load.- The relationship between simulated air load and no load for a typical group of control settings with sinusoidal table oscillation of $\pm 3.12^{\circ}$ is shown in figure 11 as plots of control-amplitude ratio K and phase angle ϵ versus angular frequency ω in radians per second. The two sets of curves contained in this figure indicate that loading the servomotor lowers the control-amplitude ratio approximately proportionally throughout the frequency range. This is accompanied by a decrease in lag at the higher frequencies.

A possible explanation of this change in phase relation between the autopilot oscillation and the resulting servomotor motion at high frequencies is that the maximum servomotor rotational velocity is attained under no-load conditions at a lower frequency than under loaded conditions. As the rate gyro can no longer increase the speed of the servomotor above this critical frequency, it is feasible that the loaded servomotor should still have an effective rate signal at higher frequencies than the unloaded motor. It follows that the loaded condition will have less lag than the unloaded case at high frequencies. The combination of the lower gearing ratio and decrease of lag for the loaded condition is to increase the dynamic stability of the model according to the criterions for stability outlined in reference 2. This increase in stability under loaded conditions was the general result noted throughout the tests.

The subsequent figures are therefore based on no-load conditions in order to make the results, from which the final servomotor linkage ratios were obtained, apply to the most critical conditions.

Effect of varying control settings.- The effect of varying the rate, range, and follow-up control settings are shown in figures 12 to 14, which are plotted for a table amplitude of $\pm 3.12^{\circ}$. These are plots of control-amplitude ratio K and phase angle ϵ versus angular frequency ω in radians per second and are typical examples of the results used to determine the optimum control settings. Optimum operating condition was selected to be the combination of control settings that would produce a

constant ratio of control (servomotor) motion per unit autopilot displacement throughout the frequency range with a minimum amount of phase-angle lag. The effect of varying rate (fig. 12) shows that high rate control settings produce a nonproportional control-amplitude ratio K with increasing frequency, while low rate settings increase the servomotor lag. The effect of varying range (fig. 13) shows that high range settings increase the servomotor lag, while low range settings make the curve of K versus frequency less proportional. The effect of varying follow-up (fig. 14) shows that decreasing the follow-up control setting causes the curve of the control-amplitude ratio versus the frequency to peak sharply and also increase the lag of the servomotor. From these tests, the control settings which give the best performance were selected to be rate 65, range 70, and follow-up 100.

Stability analysis.- The frequency-response tests of system 2 were measured for sinusoidal table frequencies of 0° to 2 cycles per second and for table amplitudes of $\pm 0.52^\circ$, $\pm 1.45^\circ$, and $\pm 3.16^\circ$ in order to predict stability for various disturbances. To determine the linkage ratios between control surface and servomotor for stable flight, frequency-response plots shown in figures 15 to 17 were made assuming unit gearing between control surface and servomotor. The model frequency-response curves (K_m and ϵ_m versus ω) for airspeeds of 300 and 850 feet per second and based on the aerodynamic data obtained in references 3 and 4 were plotted for the longitudinal and lateral planes of motion so that the stability requirements could be predicted in pitch, yaw, and roll. In pitch θ, a linkage ratio of 1° elevator control for 8° of servo motion, in roll ϕ, a linkage ratio of 1° total aileron control deflection for 12° of servo motion, and in yaw ψ, a linkage ratio of 1° rudder control for 10° servo motion will satisfy the criterion for stable flight.

Nyquist diagrams of the frequency-response curves (based on the method outlined in references 5 and 6) in which the control gearing values mentioned above were included are shown in figures 18 to 20. Since the resultant curves in figures 18 to 20 do not enclose point $(1,0^\circ)$, the critical point when NACA nomenclature for control deflection angles are used, the stability criterions are satisfied.

CONCLUSIONS

With the use of system 1, based on the action of a displacement gyroscope only, the autopilot-model combination will be longitudinally stable for disturbances in the range tested (that is, $\theta = \pm 9^\circ$, 7°, 4°, and 2°). Under normal operation, diving the model appears to start a

hunting oscillation. This hunting oscillation encountered may be eliminated by increasing the dead spot in the gyroscope pickoff from the normal value of 1.4° to 2.2°. Although doing this would change the frequency-response characteristics, the autopilot-model combination would remain stable in the amplitude range tested. Cross coupling of the autopilot was present with the pickoff in normal position. This also can be eliminated by increasing the dead spot in the gyroscope pickoff to 2.2°.

For system 2, based on the combined action of displacement and rate gyroscope, dynamic stability for the autopilot-model combination in flight can be obtained using the recommended control settings and control-surface gearings.

A comparison of the two autopilot systems shows that slight improvement in the longitudinal stability of the model can be expected when system 2 is used since the frequency response for this autopilot-model combination shows that the model will operate at a higher frequency with somewhat better damping characteristics.

Langley Aeronautical Laboratory
National Advisory Committee for Aeronautics
Langley Field, Va.

Jerome M. Teitelbaum
Aeronautical Research Scientist

Ernest C. Seaberg
Aeronautical Research Scientist

Approved:

Robert R. Gilruth
Chief of Pilotless Aircraft Research Division

Jjm

REFERENCES

1. King, L. A.: Laboratory Test of the Performance of Autopilots for 4/10-Scale Model of the Grumman F8F-1 Airplane - TED No. NACA 2466. NACA MR No. L5H03, Bur. Aero., 1945.

2. Greenberg, Harry: Frequency-Response Method for Determination of Dynamic Stability Characteristics of Airplanes with Automatic Controls. NACA TN No. 1229, 1947.

3. Cohen, Doris: Analytical Investigation of the Stability of an F8F Dropping Model with Automatic Stabilization. NACA MR No. L5L03, 1945.

4. Watson, James M., and Comisarow, Paul: Wind-Tunnel Tests of a 1/5-Scale Powered Model of the Grumman XF8F-1 Airplane. III - Lateral Stability and Control - TED No. NACA 2344. NACA MR No. L5F05, Bur. Aero., 1945.

5. James, Hubert M., Nichols, Nathaniel B., and Phillips, Ralph S.: Theory of Servomechanisms. McGraw-Hill Book Co., Inc., 1947.

6. Hall, Albert C.: The Analysis and Synthesis of Linear Servomechanisms. Servomechanisms Lab., Mass. Inst. Technology, Cambridge, Mass., 1943.

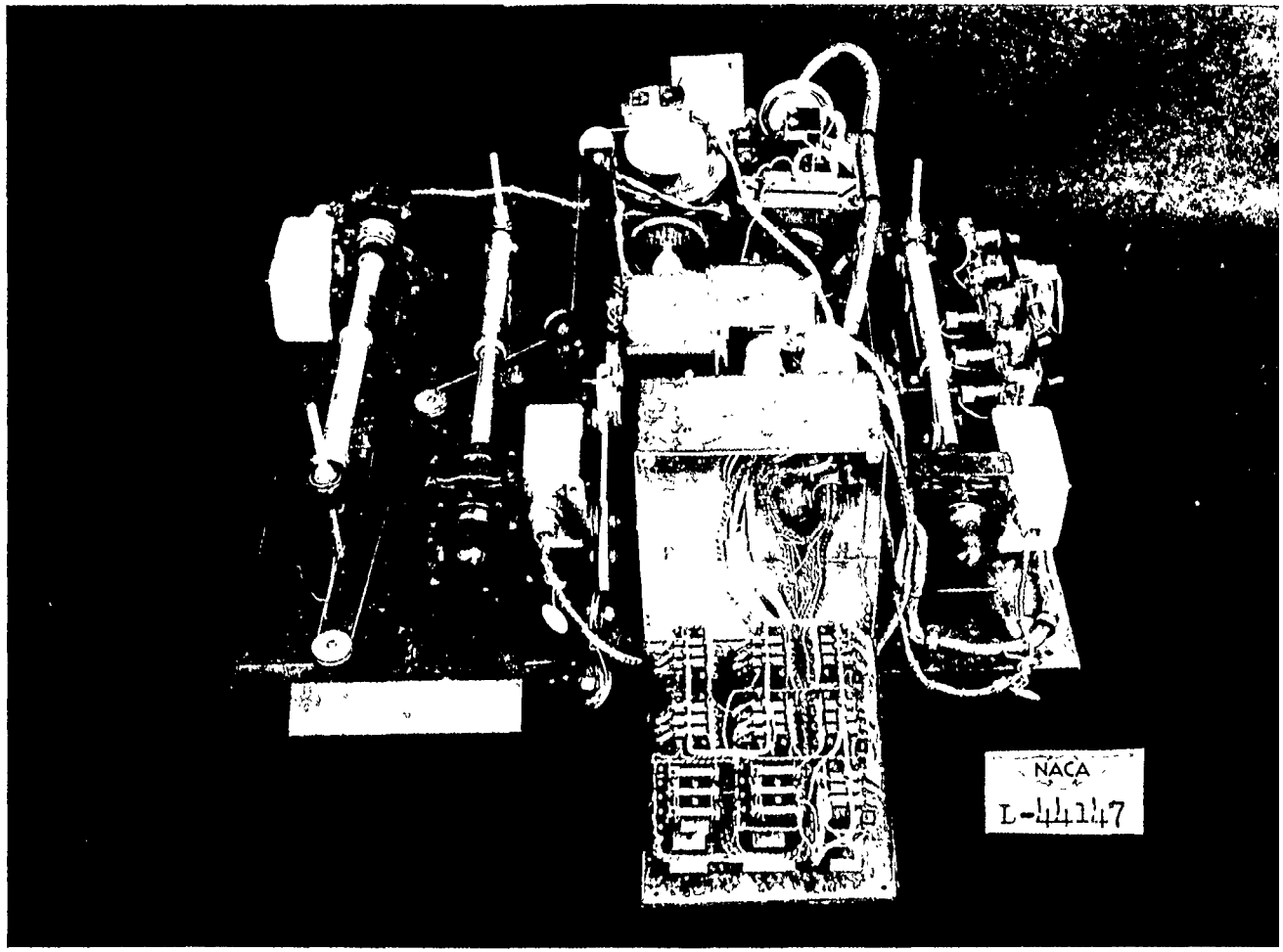

Figure 1.- System 1 autopilot for $\frac{4}{10}$-scale Grumman F8F-1 drop model.

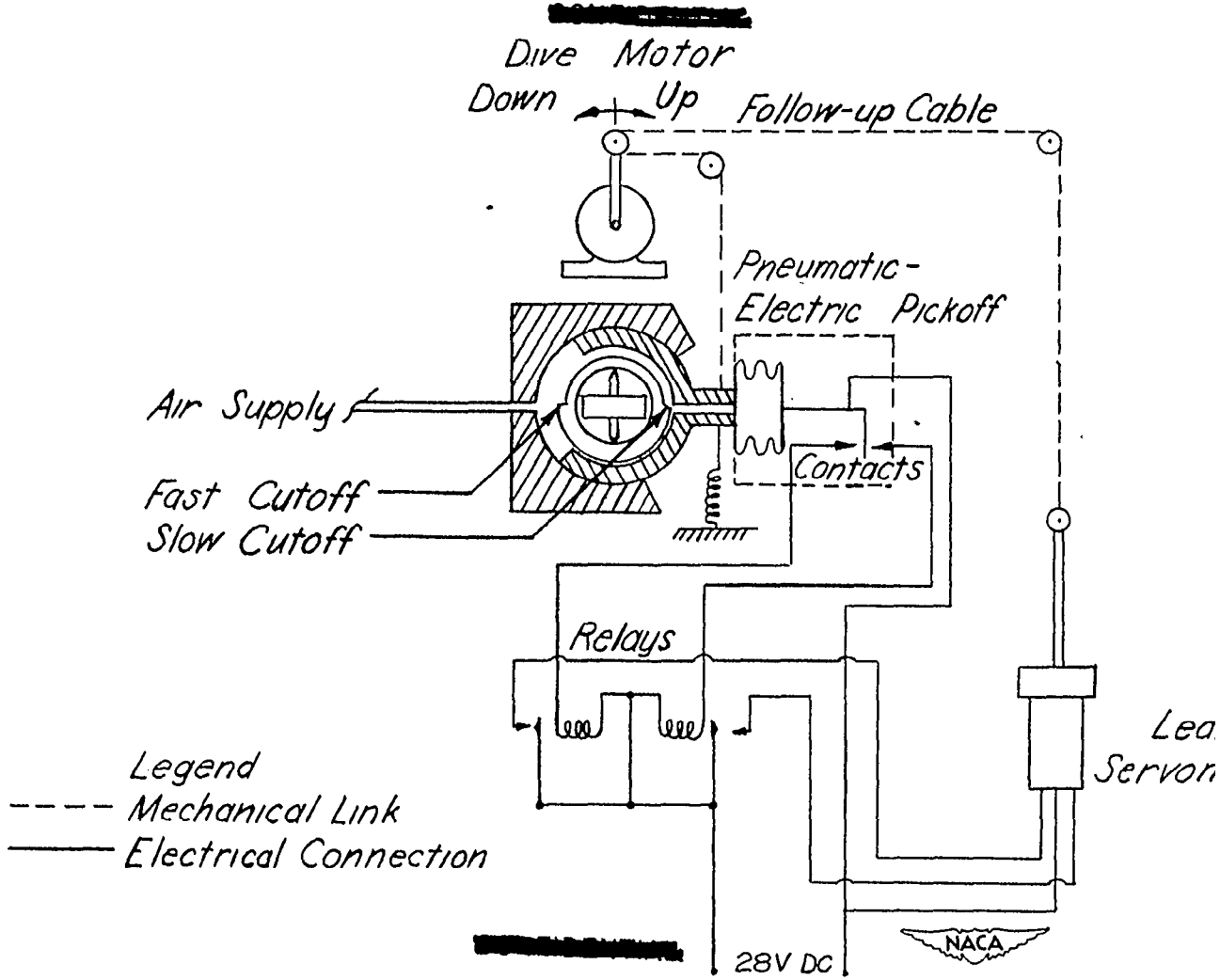

Figure 2.- Schematic diagram of system 1 autopilot for $\frac{4}{10}$-scale Grumman F8F-1 drop
One axis shown only.

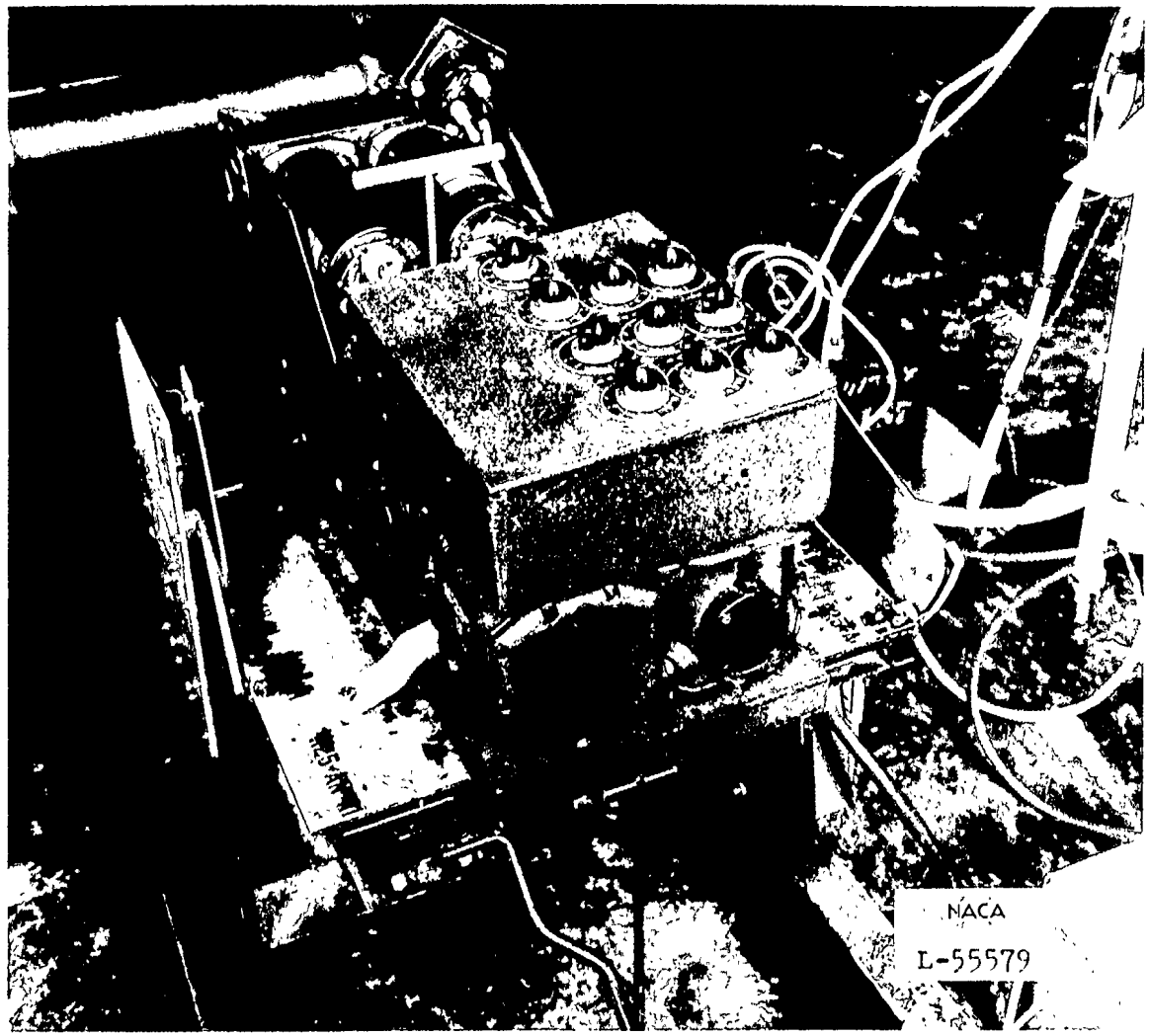

Figure 3.- System 2 autopilot for $\frac{4}{10}$-scale F8F-1 drop model as installed on oscillating table.

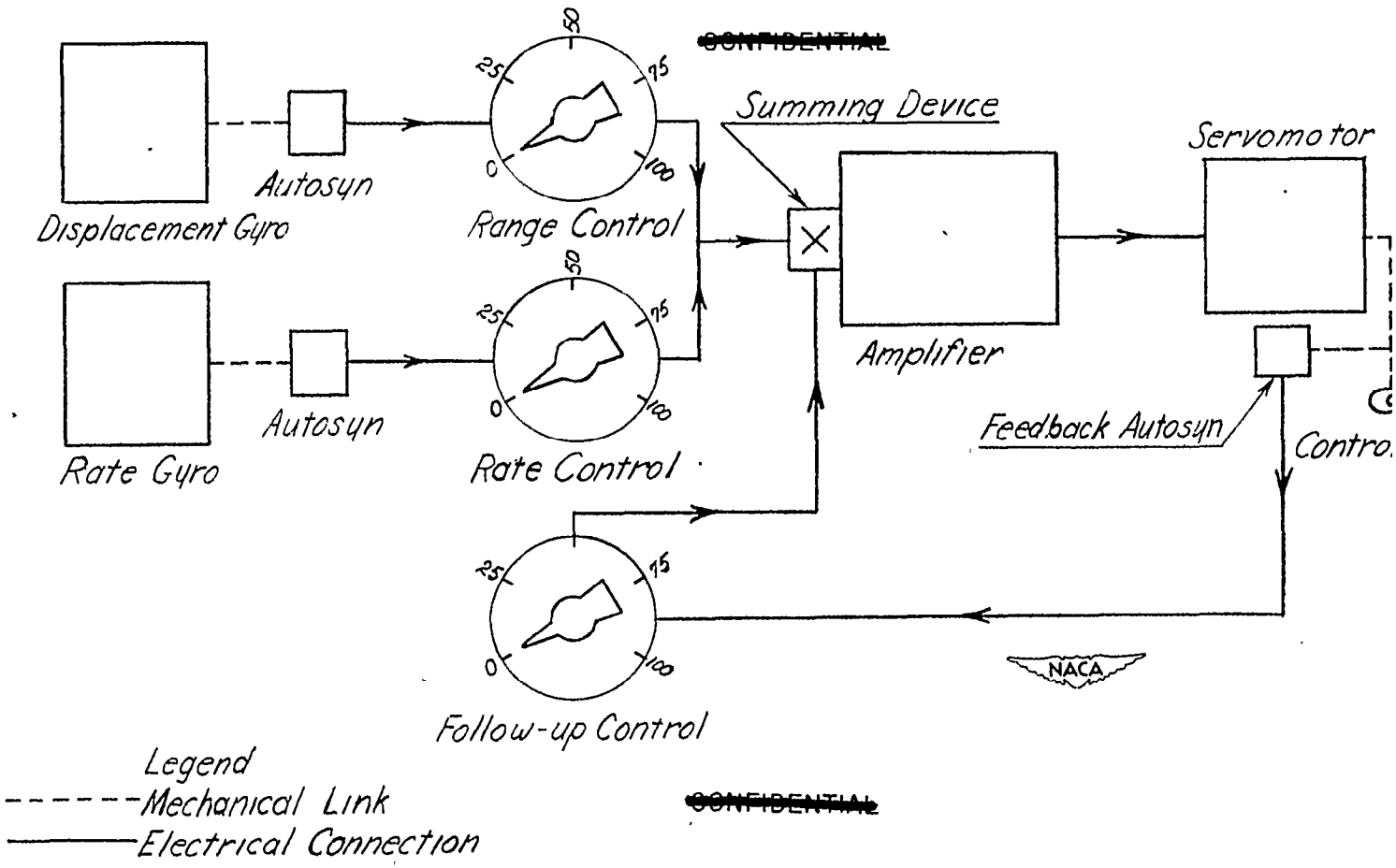

Figure 4.- Block diagram of system 2 autopilot for $\frac{4}{10}$-scale F8F-1 drop model. One axis shown

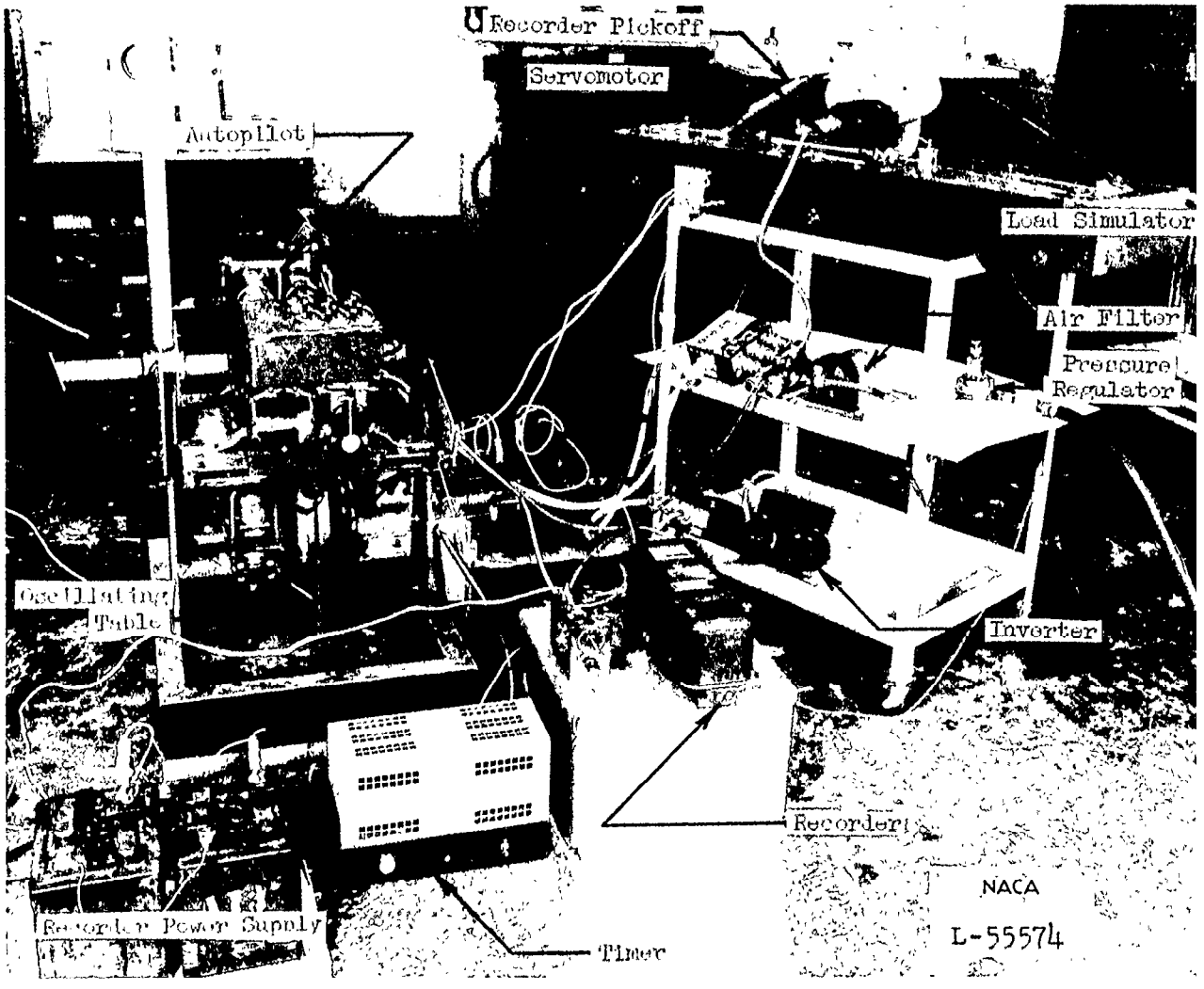

Figure 5.- Test setup used to obtain frequency response records on system 2 autopilot for $\frac{4}{10}$ F8F-1 drop model.

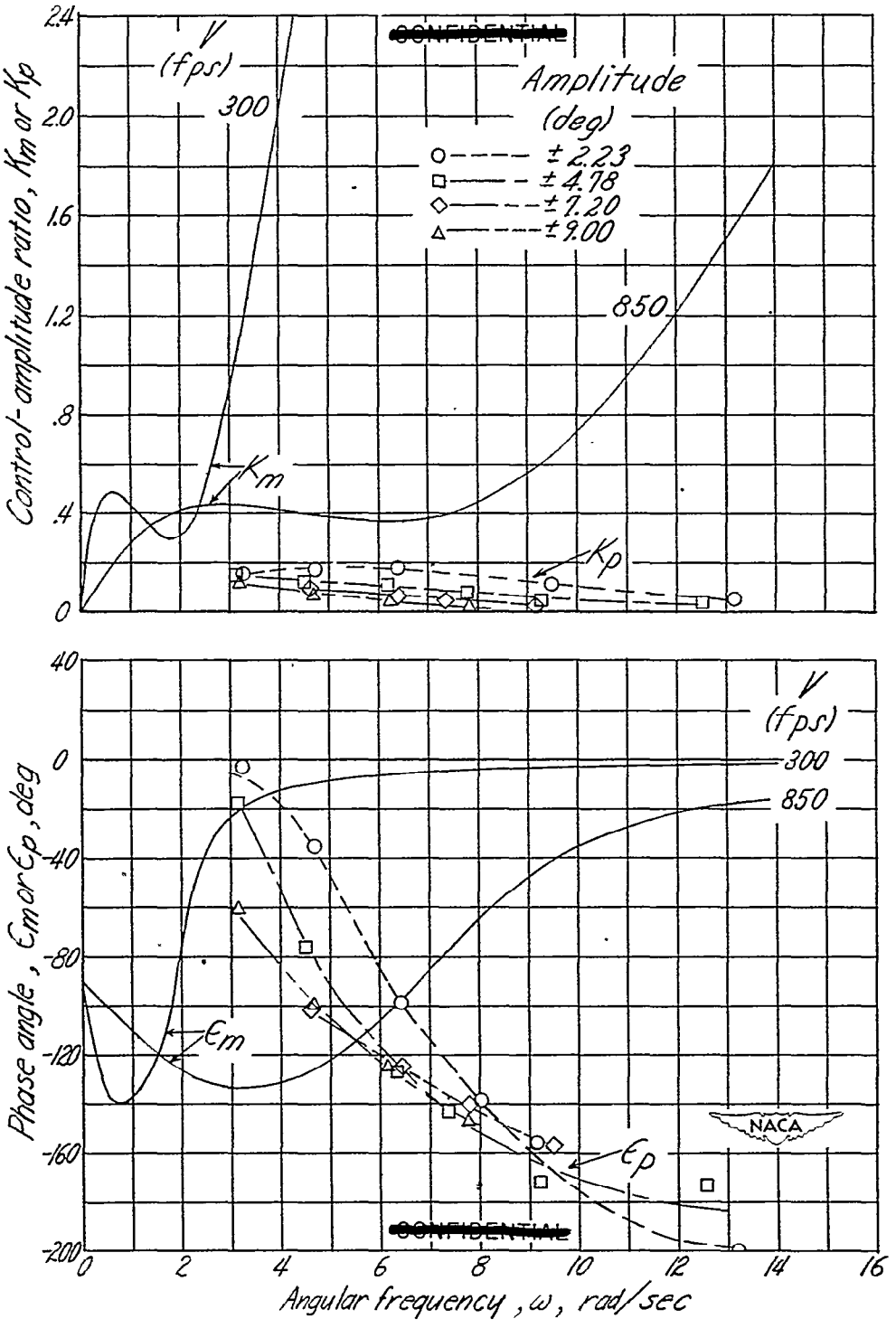

Figure 6.- Longitudinal frequency response for $\frac{4}{10}$-scale F8F-1 drop model using system 1 autopilot with normal pickoff opening.

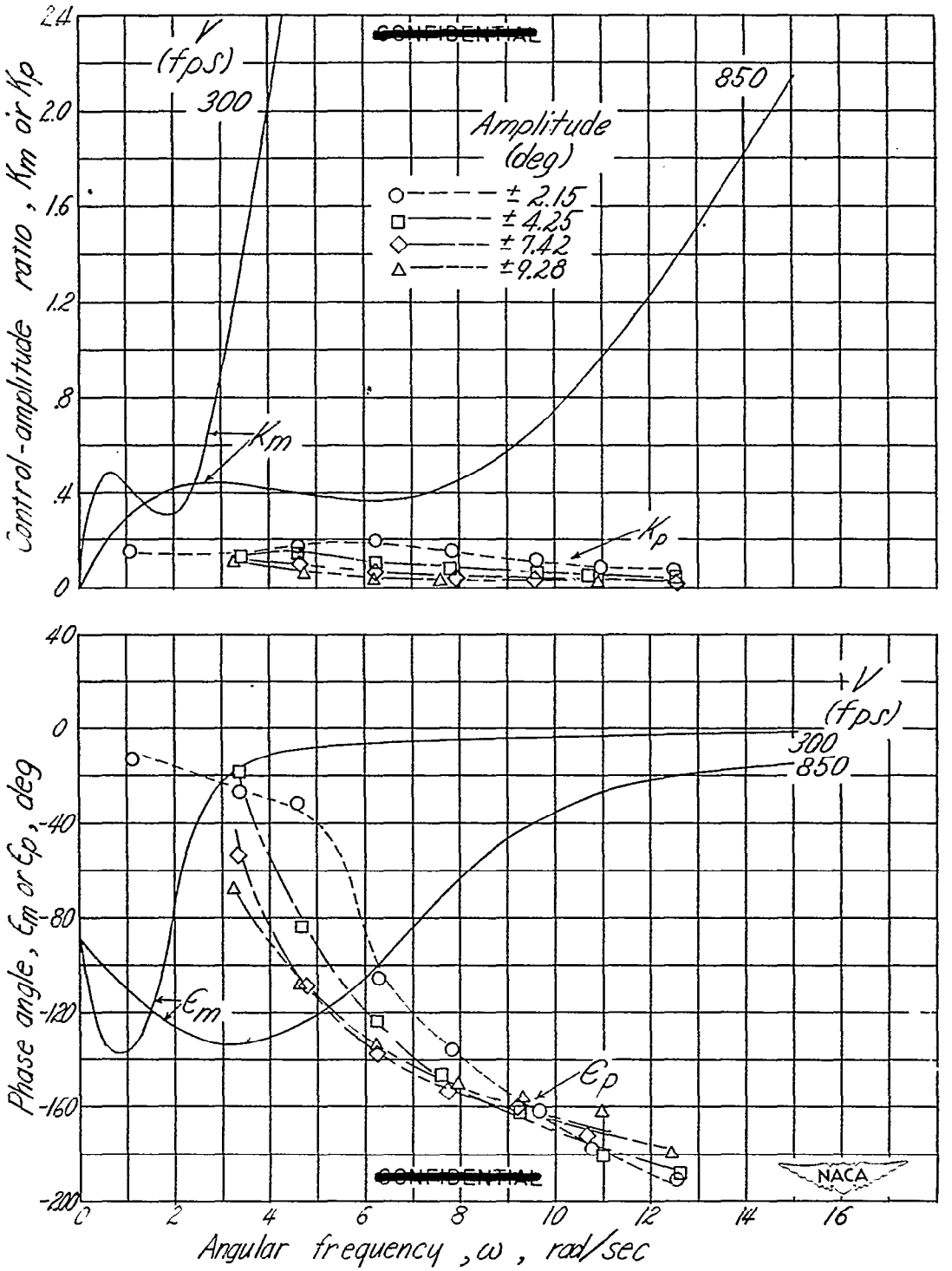

Figure 7.- Longitudinal frequency response for $\frac{4}{10}$-scale F8F-1 drop model using system 1 autopilot with pickoff in wide-open position.

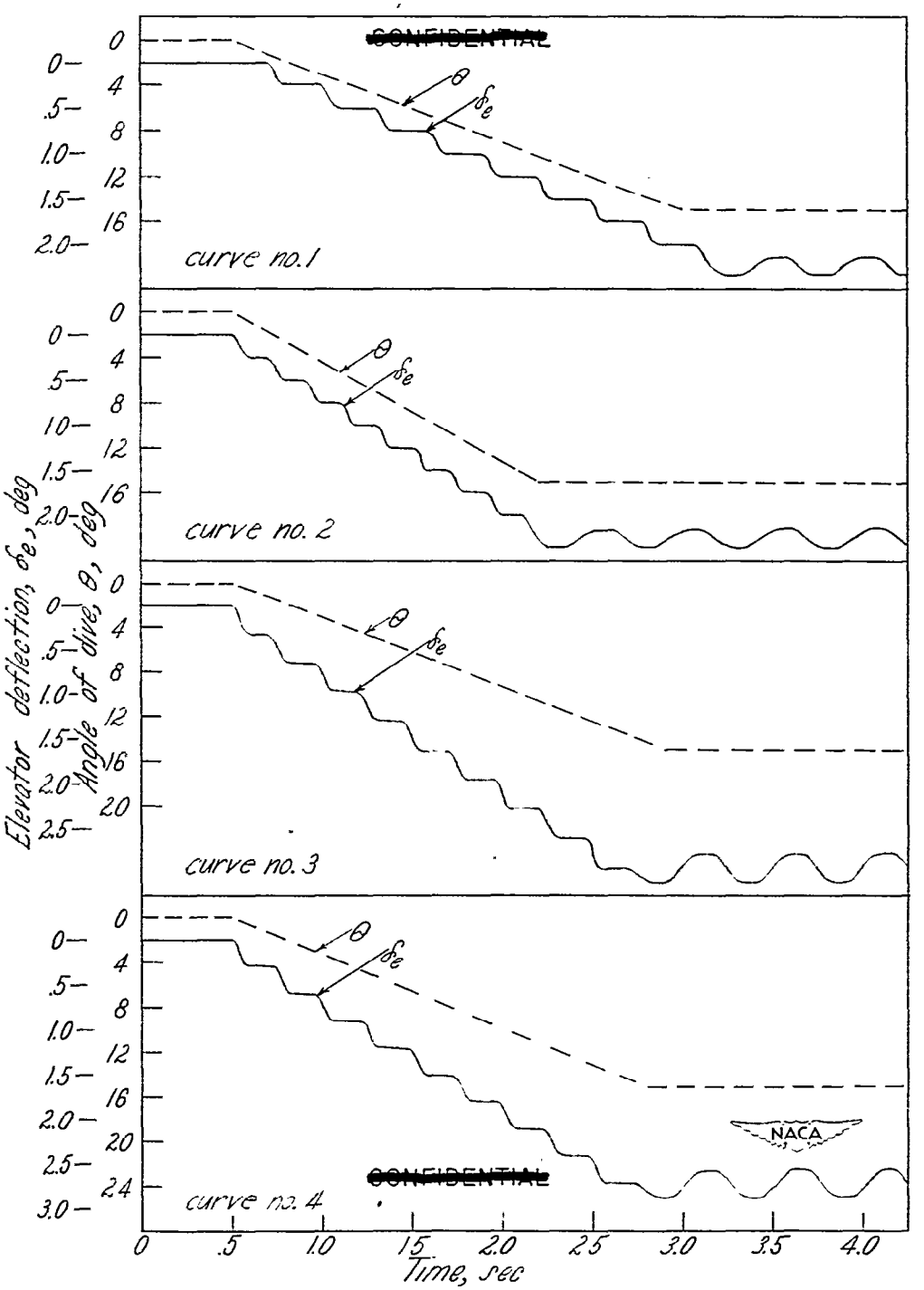

Figure 8.- Effect of dive for $\frac{4}{10}$-scale F8F-1 drop model using system 1 autopilot with normal pickoff opening. Curves Nos. 1 and 2 are with dive mechanism inoperative and curves Nos. 3 and 4 with dive mechanism in operation.

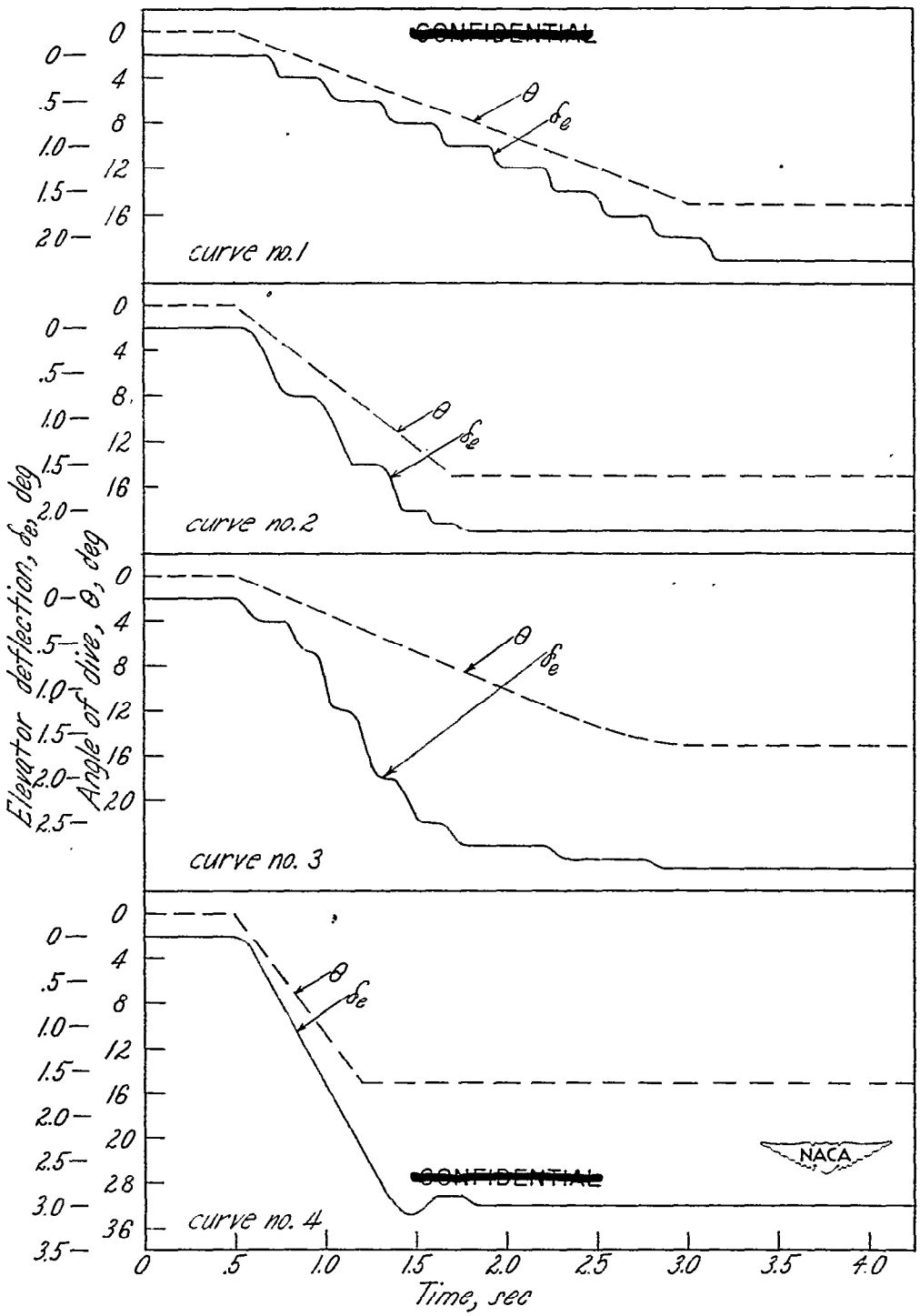

Figure 9.- Effect of dive for $\frac{4}{10}$-scale F8F-1 drop model using system 1 autopilot with pickoff in wide-open position. Curves Nos. 1 and 2 are with dive mechanism inoperative and curves Nos. 3 and 4 with dive mechanism in operation.

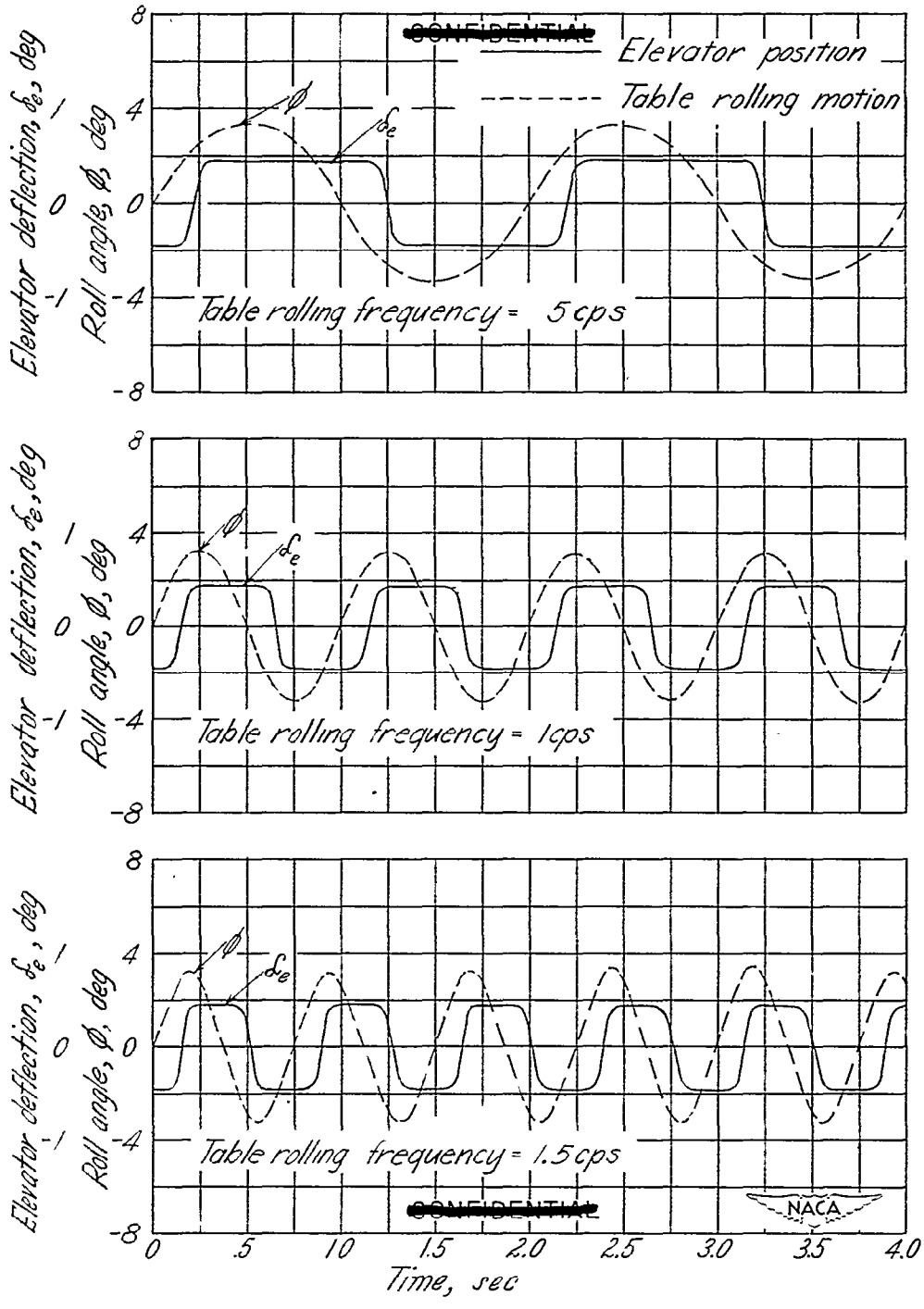

Figure 10.- Cross-coupling effect for $\frac{4}{10}$-scale F8F-1 drop model using system 1 autopilot with normal pickoff opening after a disturbance was initiated by outside source. Amplitude of table oscillation in roll of ±3.25°.

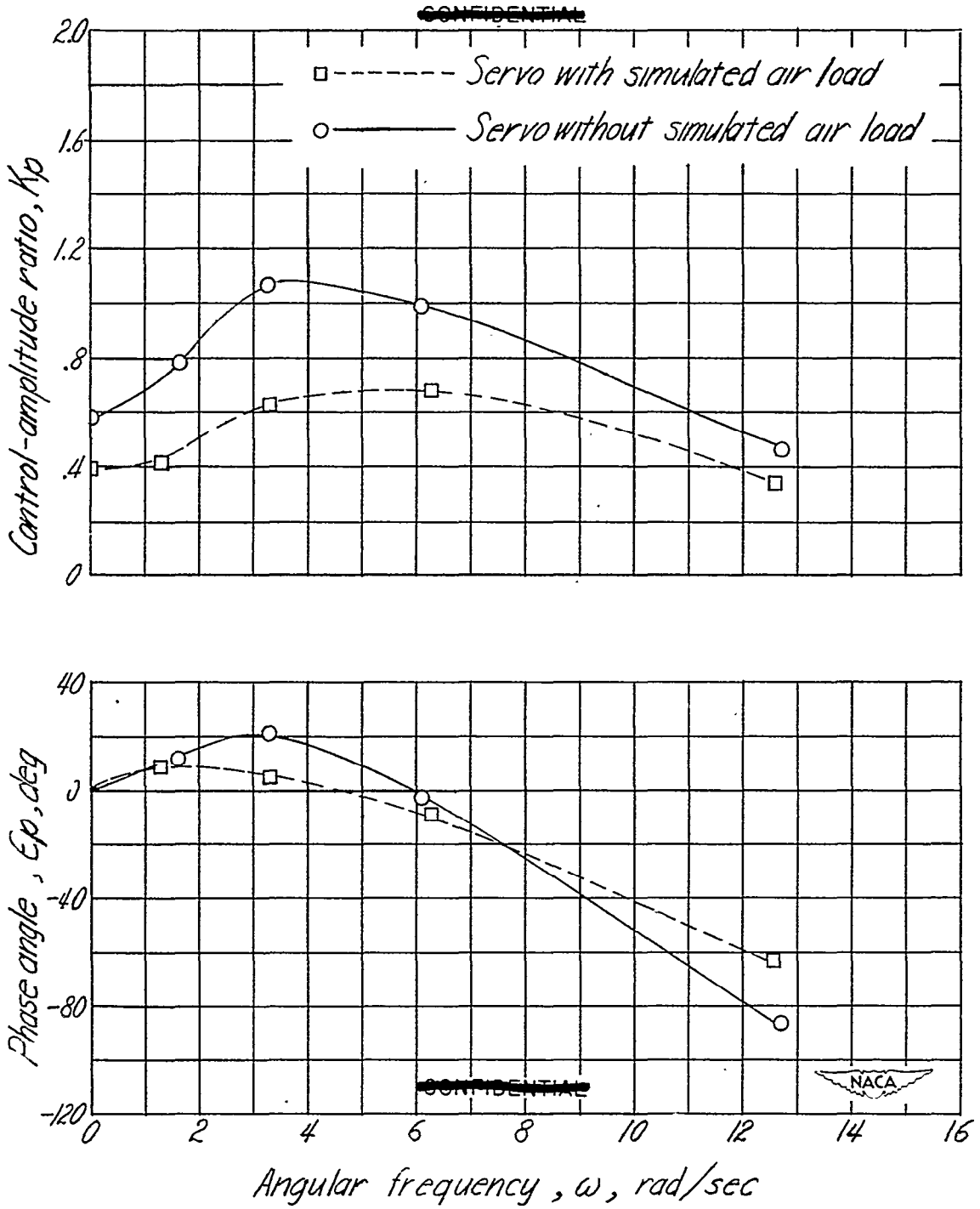

Figure 11.- Effect of loading servo on system 2 autopilot for $\frac{4}{10}$-scale F8F-1 drop model with autopilot control settings of rate 50, follow-up 100, and range 50; with simulated air load on servo of 8 to 10 foot-pounds; and with table oscillation amplitudes of $\pm 3.14^{\circ}$.

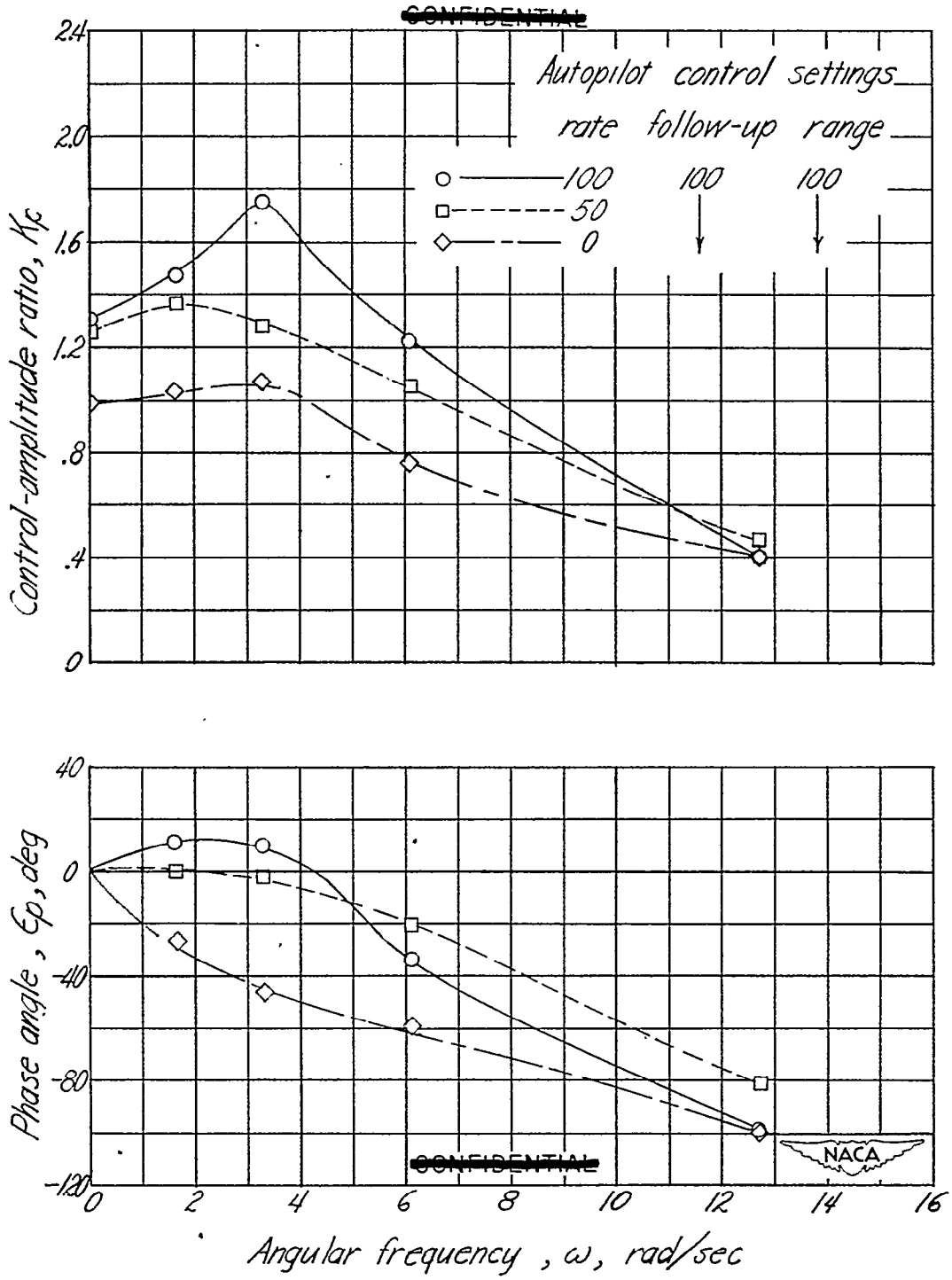

Figure 12.- Effect of variation of the rate control setting on system 2 autopilot for $\frac{4}{10}$-scale F8F-1 drop model without simulated air load on servo and with table oscillation amplitude of $\pm 3.12^{\circ}$.

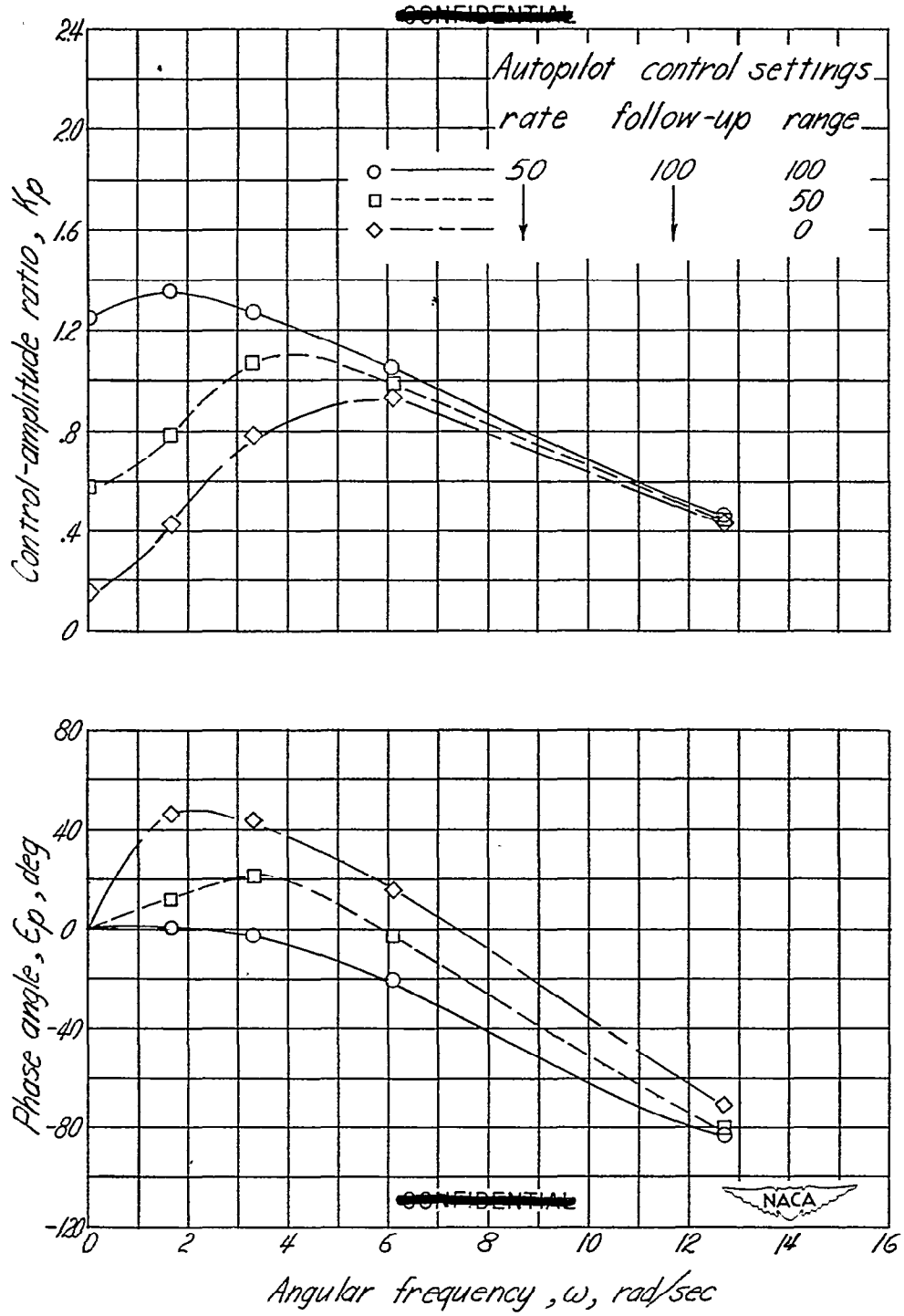

Figure 13.- Effect of variation of the range control setting on system 2 autopilot for $\frac{4}{10}$-scale F8F-1 drop model without simulated air load on servo and with table oscillation amplitude of $\pm 3.12^{\circ}$.

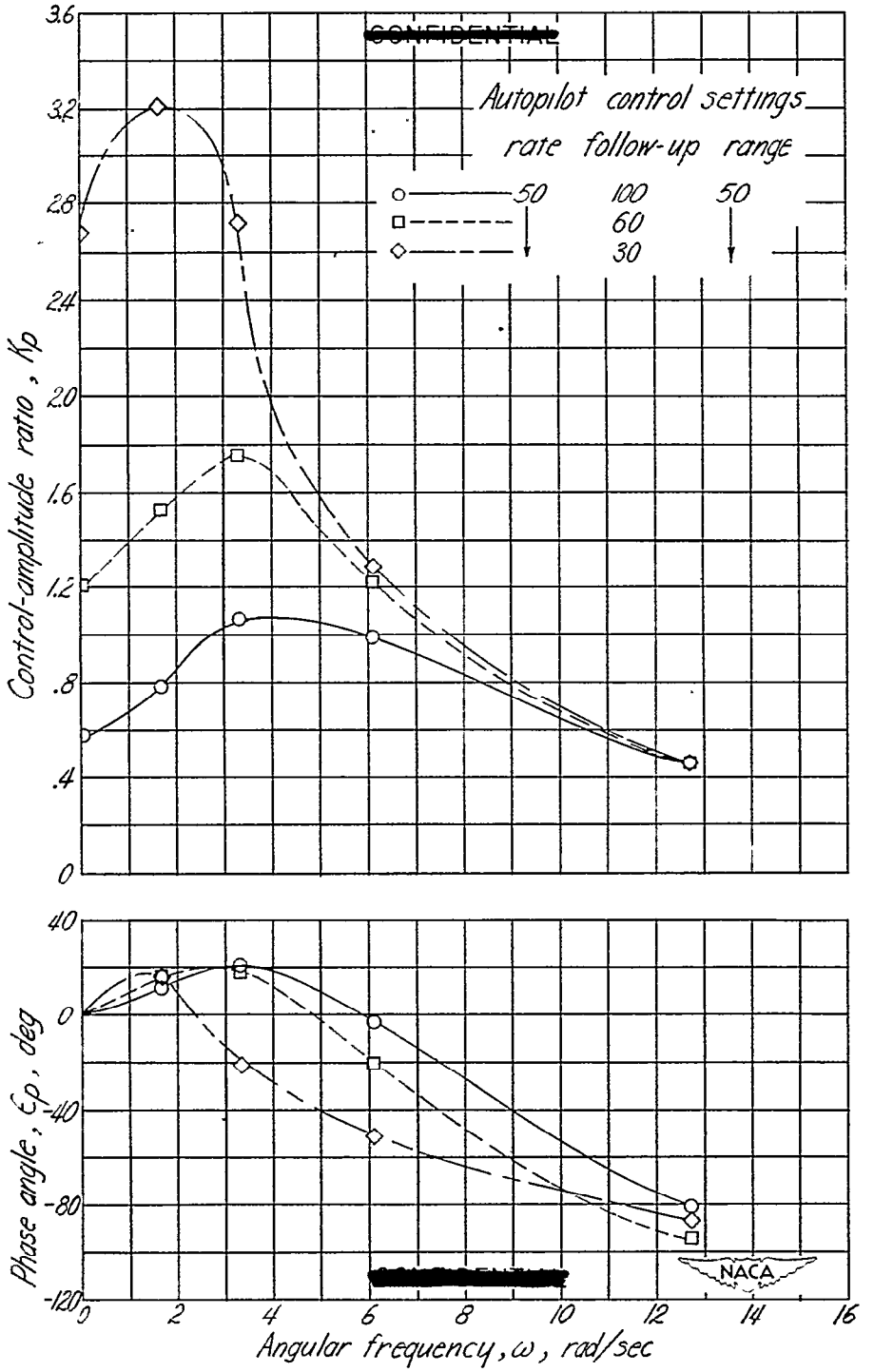

Figure 14.- Effect of variation of the follow-up control setting of system 2 autopilot for $\frac{4}{10}$-scale F8F-1 drop model without simulated air load on servo and with table oscillation amplitude of $\pm 3.12^{\circ}$.

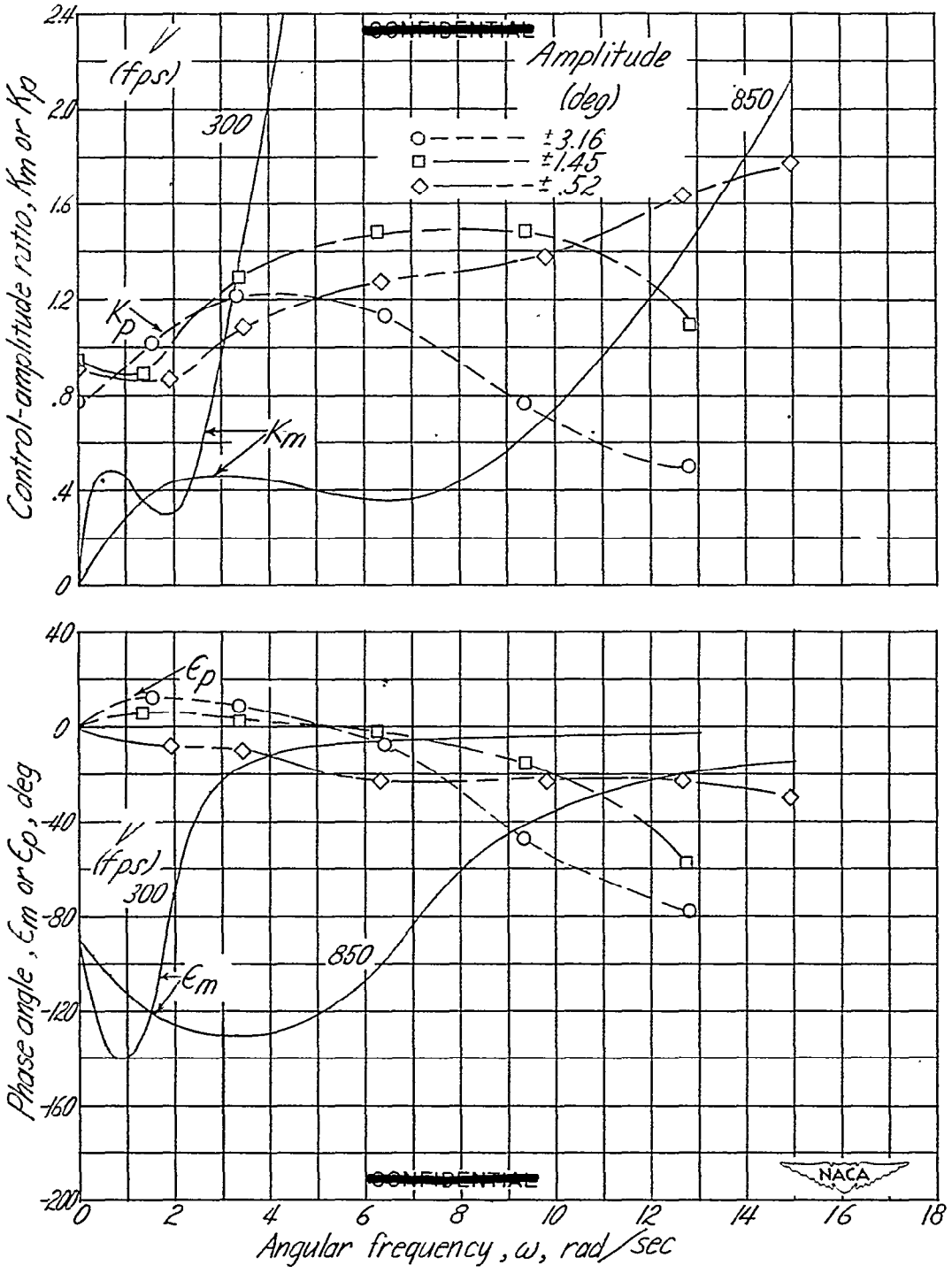

Figure 15.- Longitudinal pitch frequency response for $\frac{4}{10}$-scale F8F-1 drop model using system 2 autopilot with unit control-surface gearing ratio, without simulated air load on servo, and using autopilot control settings of rate 65, follow-up 100, and range 70.

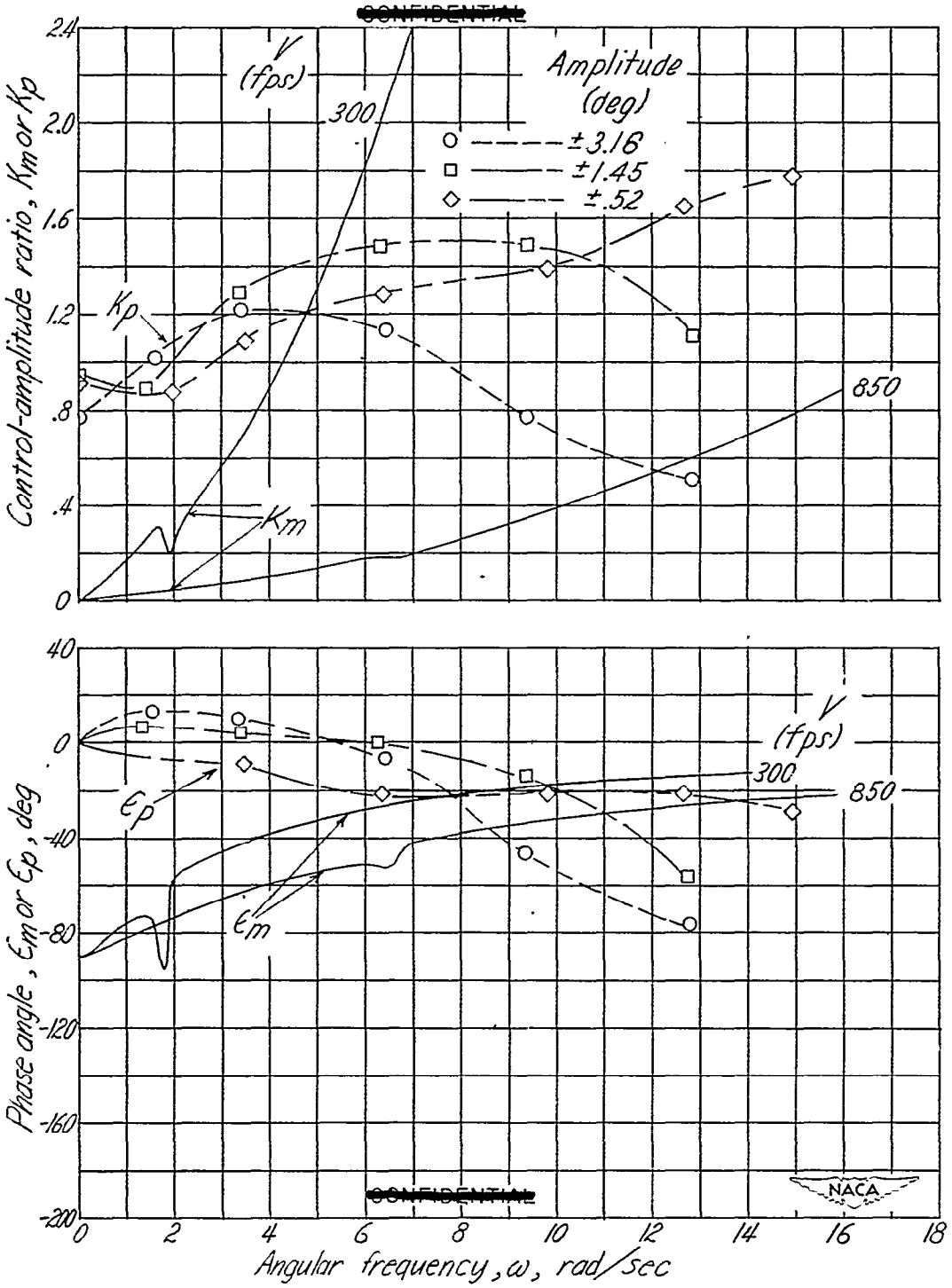

Figure 16.- Lateral roll frequency response for $\frac{4}{10}$-scale F8F-1 drop model using system 2 autopilot with unit control-surface gearing ratio, without simulated air load on servo, and using autopilot control settings of rate 65, follow-up 100, and range 70.

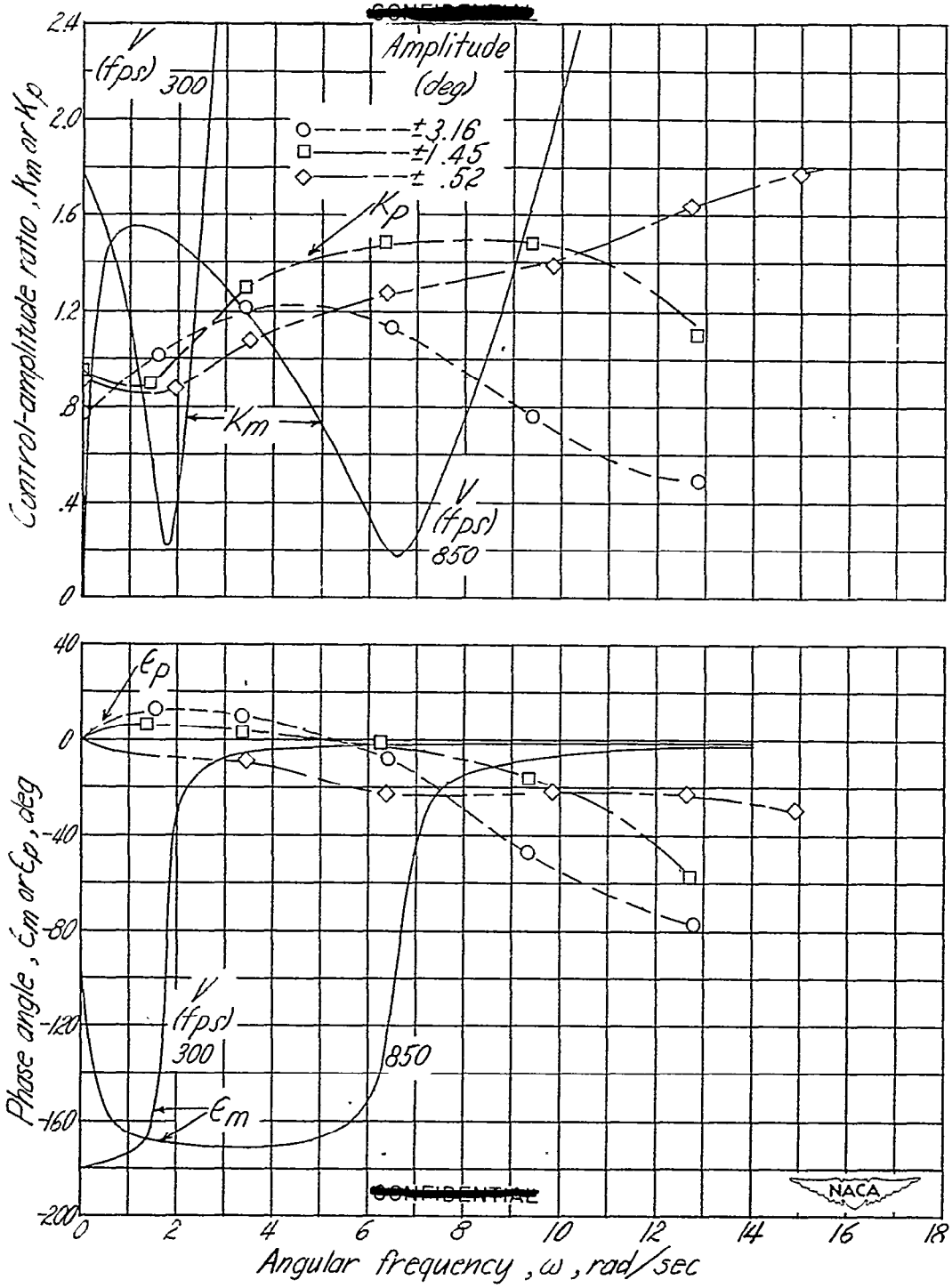

Figure 17.- Lateral yaw frequency response for $\frac{4}{10}$-scale F8F-1 model using system 2 autopilot with unit control-surface gearing ratio, without simulated air load on servo, and using autopilot control settings of rate 65, follow-up 100, and range 70.

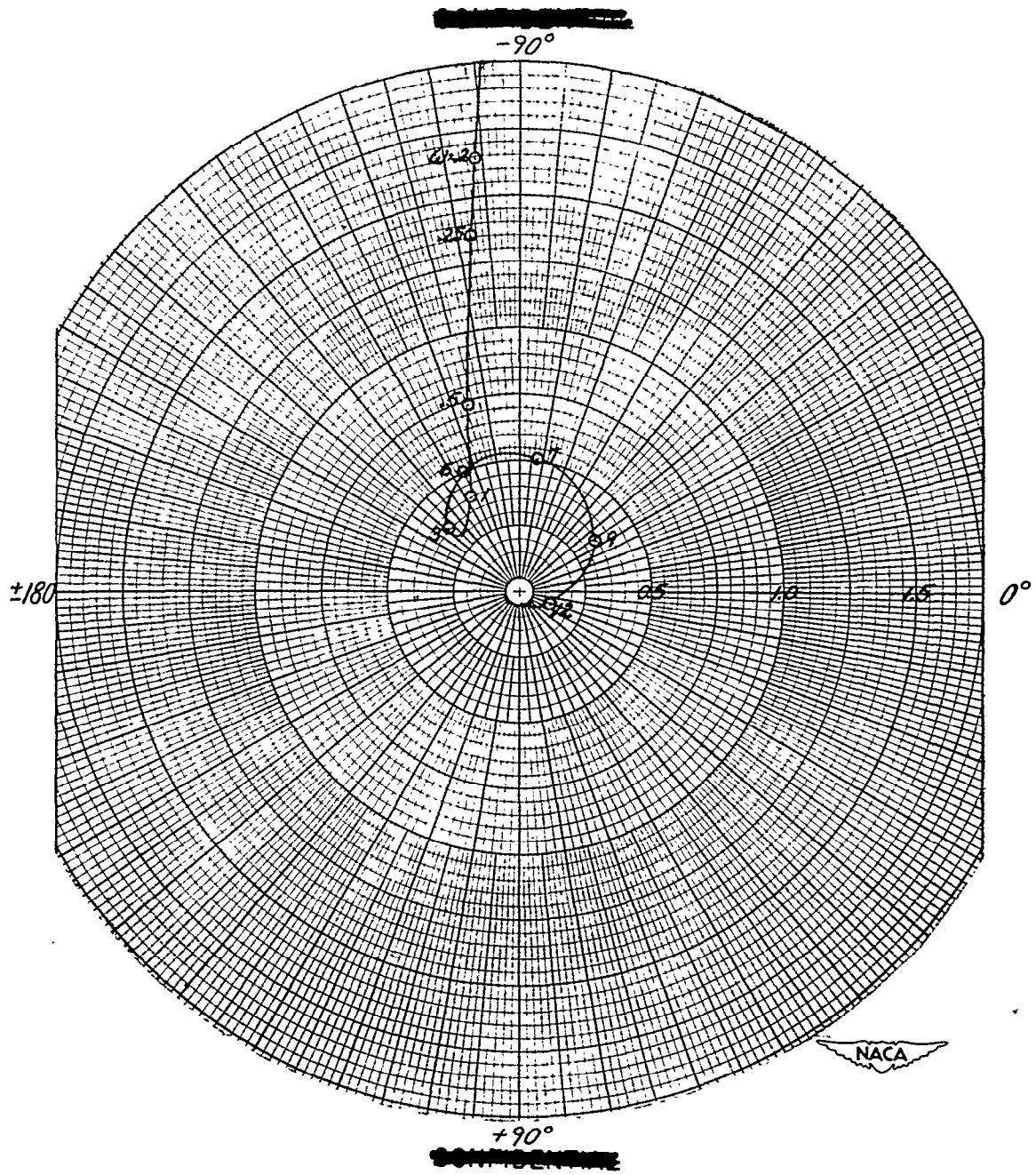

Figure 18.- Nyquist diagram for a longitudinal pitch oscillation of $\pm 1.45^{\circ}$ for the $\frac{4}{10}$-scale F8F-1 drop model assuming V = 850 feet per second and a control-surface gearing ratio of 1:8. No simulated air load and autopilot control settings of rate 65, follow-up 100, and range 70.

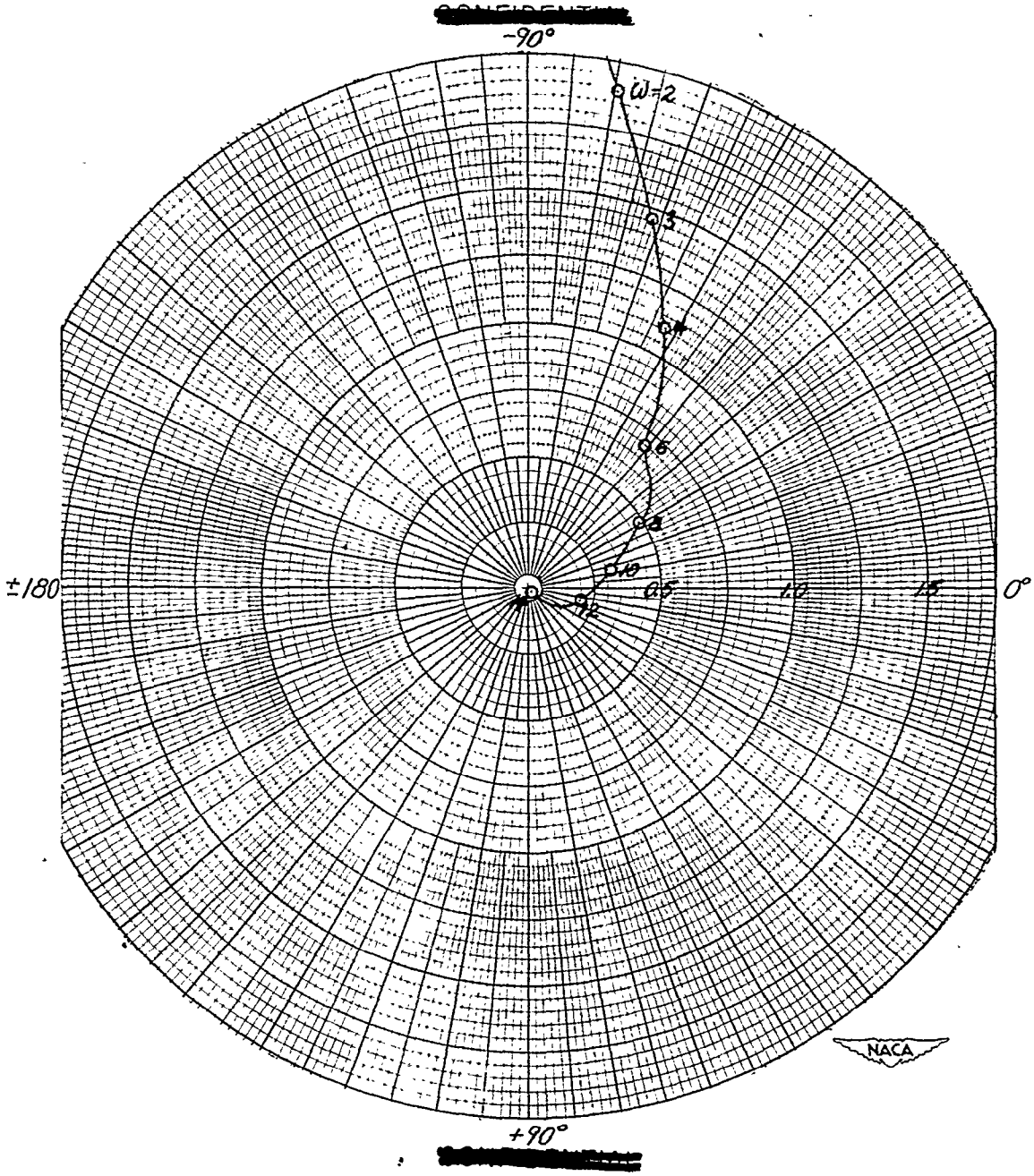

Figure 19.- Nyquist diagram for a lateral roll oscillation of ±1.45° for the $\frac{4}{10}$-scale F8F-1 drop model assuming V = 850 feet per second and a control-surface gearing ratio of 1:12. No simulated air load and autopilot control settings of rate 65, follow-up 100, range 70.

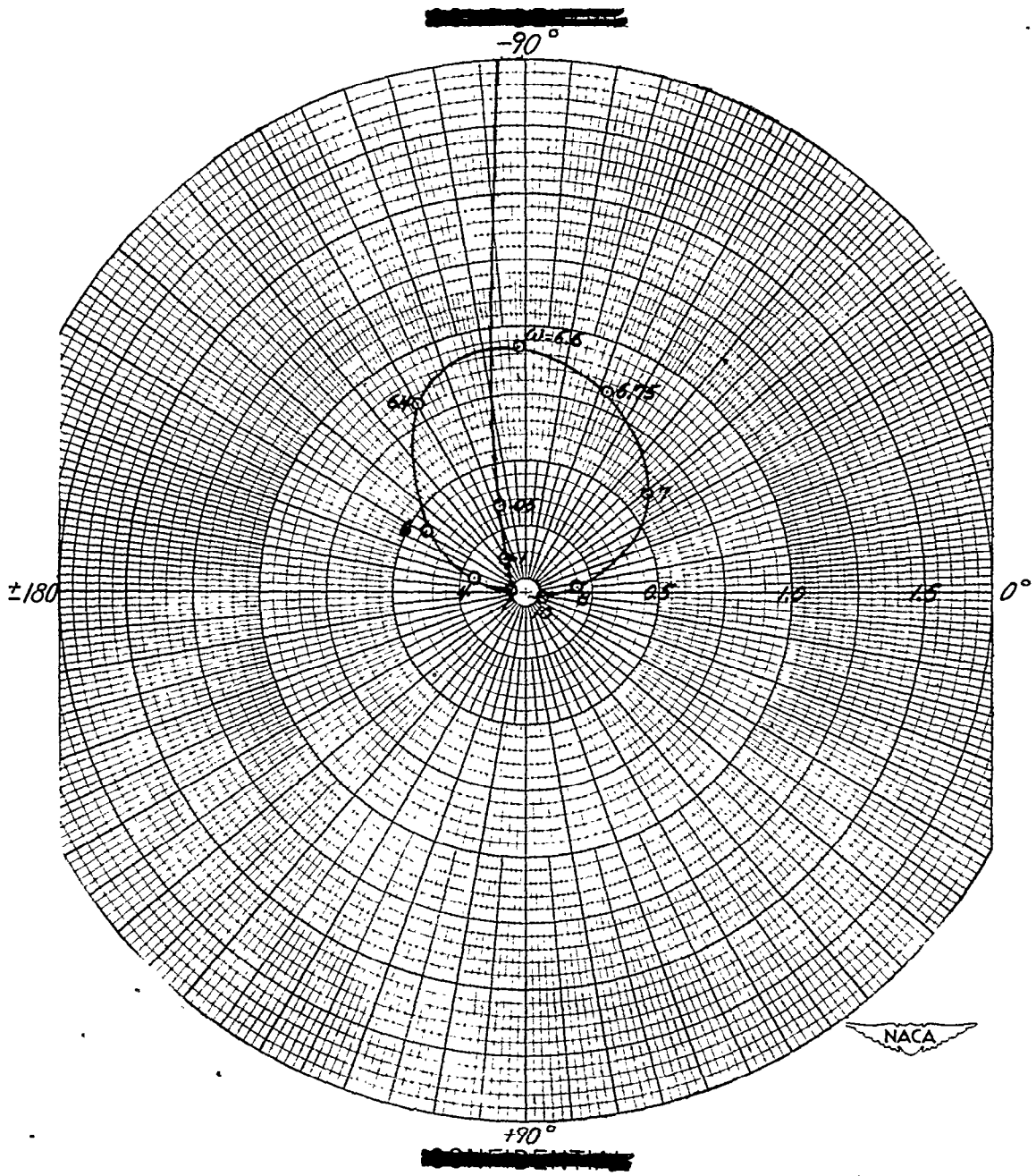

Figure 20.- Nyquist diagram for a lateral yaw oscillation of ±1.45° for the $\frac{4}{10}$-scale F8F-1 drop model assuming V = 850 feet per second and a control-surface gearing ratio of 1:10. No simulated air load and autopilot control settings of rate 65, follow-up 100, and range 70.